Adaptive modeling for free-surface flows*

Simona Perotto

MOX, Modellistica e Calcolo Scientifico
Dipartimento di Matematica "F. Brioschi"
Politecnico di Milano
via Bonardi 9
I-20133 Milano, Italy

Abstract

This work represents a first step towards the adaptive simulation of the motion of water in a complex hydrodynamic configuration, such as a channel network or a river delta by means of different mathematical models. A wide spectrum of space and time scales is involved due to the presence of physical phenomena of different nature. Ideally, moving from a hierarchy of hydrodynamic models, one should solve the most complex model (with solution u_{fine}) to accurately describe all the physical features of the problem at hand. In more detail, for a user-defined output functional $\mathcal{F}$, we aim to approximate, within a prescribed tolerance τ, the value $\mathcal{F}(u_{\text{fine}})$ by means of the quantity $\mathcal{F}(u_{\text{adapted}})$, u_{adapted} being the adapted solution confining the most complex model only on a restricted region of the computational domain. We aim to provide an efficient tool able to automatically select the regions of the domain where to solve the coarse hydrodynamic model rather than the finer one, while guaranteeing $|\mathcal{F}(u_{\text{fine}}) - \mathcal{F}(u_{\text{adapted}})|$ below the tolerance τ. This goal is achieved via a suitable *a posteriori* modeling error analysis developed in the framework of a goal-oriented theory. We extend the dual-based approach provided in [3] for steady equations to the case of a generic time-dependent problem. Then this analysis is particularized to the case of free-surface flows. In the last part of the paper an exhaustive numerical validation is carried out, while emphasizing the crucial matter of the time discretization for the dual problem.

Keywords modeling adaptivity, a posteriori error estimates, goal-oriented methods, free-surface flows, dual problem, finite elements

1 Introduction

The study of free-surface flows comprises a wide range of physical phenomena, from tidal flows, to water motion in large basins, river courses, channels, etc. Ideally, one should solve the full 3D Navier-Stokes equations to capture all the physical features of the

*This work has been supported by the GNCS Project "Numerical Methods for multiscale evolutionary problems".

problem at hand. However, this approach requires a huge computational effort. In order to reduce such a computational cost, a hierarchy of simplified hydrodynamic models has been proposed in the literature (see, e.g., [23, 25, 26]).
Essentially we can distinguish among models of different dimension (1D, 2D and 3D) and models of different physical nature, that is, derived under physical assumptions of various type. According to a dimensional classification, for the 3D case we can consider the free-surface Navier-Stokes or the hydrostatic 3D shallow water equations; concerning the 2D situation, the Boussinesq, Serre or Saint-Venant equations can be adopted; finally, in the one-dimensional case, the 1D counterparts of these latter models are usually employed. From a physical viewpoint, non-hydrostatic models (for instance, Boussinesq and Serre equations) are generally opposed to the hydrostatic ones (the Saint-Venant equations) (see Fig. 1).

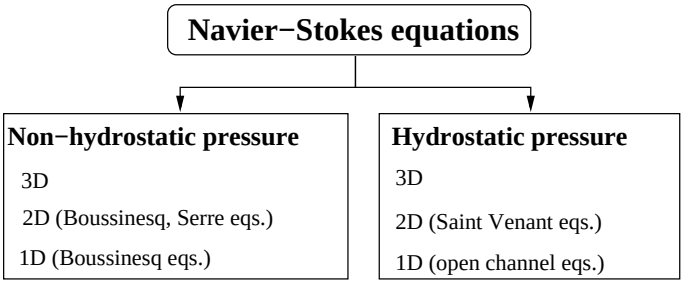

Figure 1: A possible classification of the most widespread hydrodynamic models

The approach proposed in this paper consists of a suitable coupling of some of the above mentioned models by solving the most expensive one (with solution u_{fine}) only in the regions of the domain where it is strictly necessary.
In more detail, for a user-defined output functional $\mathcal{F}$, we aim to approximate, within a prescribed tolerance τ, the value $\mathcal{F}(u_{\text{fine}})$ by means of the quantity $\mathcal{F}(u_{\text{adapted}})$, u_{adapted} being the so-called adapted solution obtained by solving the most complex model only on a restricted region of the computational domain. In particular, one can decide to couple free-surface models of different dimension (see, e.g., [14, 15]) or, alternatively, to combine models of the same dimension but different from a physical (or analytical) viewpoint. According to the model coupling classification proposed in [16], the first choice coincides with a dimensionally heterogeneous-physically homogeneous coupling, while in the second case a dimensionally homogeneous-physically heterogeneous coupling is performed. Let us exemplify these two approaches on a real hydrodynamic configuration, i.e. a river bifurcation such as that one sketched in Fig. 2. One can use a 1D model before and after the bifurcation and a 2D one in correspondence with the bifurcation (Fig. 2, on the left). Alternatively, a 2D linear model can be solved everywhere except in the region near the bifurcation where a 2D nonlinear model is adopted (Fig. 2, on the right). In both the cases the aim is to ration the more complex model.
The matter now is where are we allowed to use the simpler model and where do we have to solve the more complex one? One can make this choice *a priori*, driven, for instance,

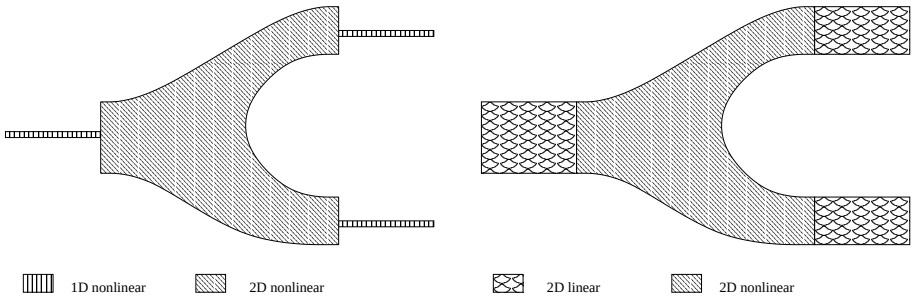

Figure 2: Sketch of a river bifurcation: coupling of a 1D nonlinear with a 2D nonlinear model (left); coupling of a 2D linear model with a 2D nonlinear one (right)

by physical considerations or, alternatively, by means of a suitable *a posteriori* modeling error estimator which can be used to automatically detect the regions where each model can be more conveniently employed. However, if the *a priori* approach is rather widespread (consider, for instance, the classical domain decomposition theory [22, 6, 21], or the geometrical multiscale approach largely investigated in the haemodynamics framework [9, 8]), the *a posteriori* analysis represents a very recent area of interest, and so far, essentially confined to dimensionally homogeneous couplings and to the modeling of heterogeneous materials [1, 17, 19, 20, 24].
Concerning the free-surface flows framework, in [14, 15] we deal with an *a priori* geometrical multiscale strategy, by coupling the 2D with the 1D shallow water models. By extending the analysis provided in [7], suitable matching conditions between the two models are derived. On the other hand the coupling of different hydrodynamics models, driven by an *a posteriori* modeling error analysis, is tackled in this paper, moving from the theory provided in [3]. A dual problem, associated with the problem at hand, is solved to measure the influence of the model on the output functional $\mathcal{F}$ of the numerical solution. This approach is a generalization to the modeling error analysis of the well-known *dual-weighted residual* method provided in [2] for the *a posteriori* discretization error control. In particular, we extend the analysis in [3] for steady equations to the case of a generic time-dependent problem. From a computational viewpoint, the main difficulty related to the unsteady problems is the time discretization of the dual problem.
The outline of the paper is as follows. In Section 2 we provide a modeling *a posteriori* error analysis for a general hierarchy of unsteady differential problems. Then, in Section 3, this analysis is particularized to the free-surface flow framework. Section 4 is devoted to the numerical discretization. Finally in Section 5 a sound numerical validation of the proposed analysis is carried out, first by introducing the adaptive procedure and then by assessing it on some significant test cases.

2 Modeling error analysis for unsteady problems

This analysis can be set in the framework of a goal-oriented adaptivity. Let $\mathcal{F}$ be the output functional we are interested in, possibly nonlinear. Standard examples of mean-

ingful functionals in Computational Fluid Dynamics (CFD) are the lift and drag around bodies in external flows or mean and local values. In the framework of free-surface flows we have considered as goal quantities essentially the kinetic energy and the vorticity of the flow on the whole or on a subregion of the computational domain (see Section 5.2).

Now, let us assume we have two time-dependent models, the *fine* model and the *coarse* one, with solution u_{fine} and u_{coarse}, respectively. At each time an "intermediate" model is solved, confining the solution of the fine model in a limited portion of the domain. This provides us with an unsteady adapted model (with solution u_{adapted}) such that $\mathcal{F}(u_{\text{adapted}})$ is an estimate for $\mathcal{F}(u_{\text{fine}})$. In this paper we derive a numerical tool able to automatically identify, at each time, the regions of the domain where the two models have to be solved, so that the quantity $|\mathcal{F}(u_{\text{fine}}) - \mathcal{F}(u_{\text{adapted}})|$ be under a prescribed tolerance, while minimizing the computational cost. Such a task is achieved via a suitable *a posteriori* modeling error analysis, i.e. by controlling $\mathcal{F}(u_{\text{fine}}) - \mathcal{F}(u_{\text{adapted}})$ in terms of quantities cheap to compute.
The reference *a posteriori* analysis is the dual-based approach proposed in [3].

Throughout we use a standard notation to denote the Sobolev spaces of functions with Lebesgue measurable derivatives, and the corresponding norms [12].

Let $Q = \Omega \times (0, T]$ be the considered space-time domain, with Ω an open (regular) bounded set of $\mathbb{R}^d$, with $d = 1, 2, 3$, and $T > 0$. Let us introduce the following *family* of primal problems in variational formulation: find $u_\alpha \in V$ such that

$$\Big(\frac{\partial u_\alpha}{\partial t}, \psi\Big) + a(u_\alpha)(\psi) + d(u_\alpha)(\alpha\psi) = (f, \psi), \qquad \text{for any } \psi \in V, \tag{1}$$

with $u_\alpha(0) = u_\alpha^0$, u_α^0 being the initial datum, and with $f \in L^2(Q)$ a given function. Here V is a suitable space-time functional space accounting for the boundary conditions associated with the problem at hand, while $(\cdot, \cdot)$ is the standard $L^2(Q)$-scalar product. The quantities $a(u_\alpha)(\cdot)$ and $d(u_\alpha)(\cdot)$ in (1) denote semilinear forms, i.e. they are linear with respect to the second argument but *may be* nonlinear in u_α. Moreover, let us assume the form $d(u_\alpha)(\cdot)$ to be "trickier" than $a(u_\alpha)(\cdot)$ from an analytical viewpoint.
The parameter $\alpha = \alpha(\mathbf{x}, t) \in L^\infty(Q)$ in (1), with $\mathbf{x} = (x, y)^T \in \Omega$ and $t \in (0, T]$, is a function, piecewise constant on a given partition of Q in subdomains Q_i and taking on only the values 0 and 1. In view of the discrete formulation, the partition $\{Q_i\}$ of Q can be identified with the computational space-time grid.
In particular, the choice $\alpha = 1$ everywhere yields the *fine* problem (i.e. the most difficult one) on the whole domain, while for α identically equal to zero we switch to the *coarse* model (i.e. to the simplest one). In practice, at each time t_j, according to the information provided by the modeling error estimator, we compute the solution of an intermediate primal problem (1) with the trickier part $d(u_\alpha)(\psi)$ "active" only in the subdomains Q_i of Ω where $\alpha(\mathbf{x}, t_j) = 1$, with $\mathbf{x} \in Q_i$. Notice that, even if we get rid of the semilinear form $d(u_\alpha)(\psi)$ in some areas of the domain, we are neither changing the differential nature of problem (1) nor the associated boundary conditions. Thus the functional space V is the same for each model of the family (1).

Remark 2.1 *The choice of the coarse model can be driven by different strategies. Ideally, a hierarchy of models describing the phenomenon we are interested in should be available. Then, one can choose a coarse model simpler, for instance, from an analytical point of view (a coarse linear problem instead of a fine nonlinear one) or from a physical viewpoint (e.g., a mathematical model derived under simplifying physical hypotheses). For instance, in the elasticity framework, the most recurrent choice consists of substituting the elasticity tensor (usually a highly oscillatory function of the position) with a regularized elasticity tensor, obtained through some homogenization process (see [17, 18, 19, 20]). In Section* 3 *we specify the criterion that we have adopted for free-surface flow problems.*

Let us begin by analyzing the *fine* primal problem. The corresponding variational formulation is given by (1) with $\alpha = 1$, and reads as: find $u_1 \in V$ such that

$$\Big(\frac{\partial u_1}{\partial t}, \psi\Big) + a(u_1)(\psi) + d(u_1)(\psi) = (f, \psi), \qquad \text{for any } \psi \in V, \tag{2}$$

with $u_1(0) = u_1^0$ the initial datum.
Let us assume that the solution u_1 of (2) exists unique in V. This hypothesis allows us to introduce the following trivial constrained minimization problem, according to an optimal control approach [2, 3, 17]: find $u_1 \in V$ such that

$$\mathcal{F}(u_1) = \inf_{v \in M} \mathcal{F}(v), \tag{3}$$

where

$$M = \Big\{ v \in V \ : \ \Big(\frac{\partial v}{\partial t}, \xi\Big) + a(v)(\xi) + d(v)(\xi) = (f, \xi), \text{ for any } \xi \in V, \text{ and with } v(0) = u_1^0 \Big\},$$

$\mathcal{F}$ being the chosen goal output functional, defined on V. The minimum u_1 of (3) coincides with the first component of the saddle point $x_1 = (u_1, z_1) \in X = V \times V$ of the *fine* Lagrangian

$$L(x_1) = \mathcal{F}(u_1) + (f, z_1) - a(u_1)(z_1) - d(u_1)(z_1) - \Big(\frac{\partial u_1}{\partial t}, z_1\Big), \tag{4}$$

z_1 being the Lagrange multiplier (or influence function) associated with the functional $\mathcal{F}$. The critical point x_1 of L is such that

$$L'(x_1)(y) = 0, \qquad \text{for any } y = (\varphi, \psi) \in X, \tag{5}$$

where

$$\begin{aligned} L'(x_1)(y) \ &= \ \mathcal{F}'(u_1)(\varphi) - a'(u_1)(\varphi, z_1) - d'(u_1)(\varphi, z_1) - \Big(\frac{\partial \varphi}{\partial t}, z_1\Big) \\ &+ \ (f, \psi) - a(u_1)(\psi) - d(u_1)(\psi) - \Big(\frac{\partial u_1}{\partial t}, \psi\Big) \end{aligned} \tag{6}$$

denotes the derivative of the fine Lagrangian L applied to the test function y. Notice that in (6) we resort to a Gâteaux differentiation, L being a differentiable functional on X [13]. Thus, the semilinear forms

$$\mathcal{F}'(u_1)(\varphi) = \lim_{\theta \to 0} \frac{1}{\theta} \{\mathcal{F}(u_1 + \theta\varphi) - \mathcal{F}(u_1)\}, \tag{7}$$

$$a'(u_1)(\varphi, z_1) = \lim_{\theta \to 0} \frac{1}{\theta} \{a(u_1 + \theta\varphi)(z_1) - a(u_1)(z_1)\}, \tag{8}$$

$$d'(u_1)(\varphi, z_1) = \lim_{\theta \to 0} \frac{1}{\theta} \{d(u_1 + \theta\varphi)(z_1) - d(u_1)(z_1)\} \tag{9}$$

are linear with respect to φ and z_1 but preserve the nonlinearity in u_1.
Via (5)-(6), the minimization problem (3) can be solved by looking for $x_1 = (u_1, z_1) \in X$ such that

$$\Big(\frac{\partial u_1}{\partial t}, \psi\Big) + a(u_1)(\psi) + d(u_1)(\psi) = (f, \psi), \qquad \text{for any } \psi \in V, \tag{10}$$

$$\Big(\frac{\partial \varphi}{\partial t}, z_1\Big) + a'(u_1)(\varphi, z_1) + d'(u_1)(\varphi, z_1) = \mathcal{F}'(u_1)(\varphi), \qquad \text{for any } \varphi \in V, \tag{11}$$

with $u_1(0) = u_1^0$. We recognize in (10) the variational formulation (2) of the fine primal problem, while equation (11) coincides with the fine dual problem, associated with (2), and corresponding to the choice $\mathcal{F}$ for the goal quantity. Notice that the dual problem (11) is linear with respect to the influence function z_1. Moreover it will be completed with a suitable final condition $z_1(T) = z_1^T$.

Now, let us identify equation (1) with the variational formulation of the *adapted* primal problem.
The constrained minimization problem (3) is thus replaced by the new one: find $u_\alpha \in V$ such that

$$\mathcal{F}(u_\alpha) = \inf_{v \in M_\alpha} \mathcal{F}(v), \tag{12}$$

where

$$M_\alpha = \Big\{ v \in V \ : \ \Big(\frac{\partial v}{\partial t}, \xi\Big) + a(v)(\xi) + d(v)(\alpha\xi) = (f, \xi), \text{ for any } \xi \in V, \text{ and with } v(0) = u_\alpha^0 \Big\}.$$

We introduce the *adapted* Lagrangian

$$L_\alpha(x_\alpha) = \mathcal{F}(u_\alpha) + (f, z_\alpha) - a(u_\alpha)(z_\alpha) - d(u_\alpha)(\alpha z_\alpha) - \Big(\frac{\partial u_\alpha}{\partial t}, z_\alpha\Big), \tag{13}$$

$x_\alpha = (u_\alpha, z_\alpha) \in X$ and z_α being the saddle point of L_α and the Lagrange multiplier associated with the functional $\mathcal{F}$, respectively. By repeating exactly the same procedure used for the fine problem, we reformulate (12) as the search of the solution u_α of the adapted primal problem (1) together with the solution of the adapted dual problem

$$\Big(\frac{\partial \varphi}{\partial t}, z_\alpha\Big) + a'(u_\alpha)(\varphi, z_\alpha) + d'(u_\alpha)(\varphi, \alpha z_\alpha) = \mathcal{F}'(u_\alpha)(\varphi), \qquad \text{for any } \varphi \in V, \tag{14}$$

with $z_\alpha(T) = z_\alpha^T$.

Remark 2.2 *The dual problems (11) and (14) have to be provided with suitable boundary conditions. In the steady case and for an output functional $\mathcal{F}$ consisting of an integral over the whole domain Ω and of an integral on the boundary $\partial\Omega$ of the domain, the dual boundary conditions can be rigorously identified according to the analysis in [10]. In the model adaption framework, a first attempt in such a direction has been performed in [4] for a relatively simple problem, the one-dimensional Helmholtz equation. On the other hand, in the presence of time-dependent problems or for more complex functionals $\mathcal{F}$, it is rather standard to provide the dual problem with the same boundary conditions as the primal problem, after a suitable homogenization (see, e.g., [2]). The dual space is thus identified with the primal one. This is the choice made in the sequel in the free-surface flow framework.*

In the sequel the notations are shortened thanks to the trivial relation between the fine and the adapted Lagrangians, i.e.

$$L(x) = L_\alpha(x) + \delta L(x), \qquad \text{for any } x = (u, z) \in X, \tag{15}$$

with

$$\delta L(x) = -d(u)((1-\alpha)z). \tag{16}$$

With the aim of keeping the quantity $\mathcal{F}(u_1) - \mathcal{F}(u_\alpha)$ below a prescribed tolerance, let us first remark that relations (4) and (13) provide us with the exact values

$$\mathcal{F}(u_1) = L(x_1) \qquad \text{and} \qquad \mathcal{F}(u_\alpha) = L_\alpha(x_\alpha), \tag{17}$$

i.e. $\mathcal{F}(u_1)$ and $\mathcal{F}(u_\alpha)$ coincide with the values of the fine and of the adapted Lagrangians at the stationary points x_1 and x_α, respectively. On the other hand, we would like to skip the approximation of the fine problem: thus we look for an estimate of the quantity $\mathcal{F}(u_1) - \mathcal{F}(u_\alpha)$ in terms of easily computable quantities, i.e. of the data problem and of the adapted solutions u_α and z_α only. With this aim, let us define the *modeling residuals* $\rho_M(u_\alpha)(\psi)$ and $\overline{\rho}_M(u_\alpha)(\varphi, z_\alpha)$ associated with the fine primal and dual problem, respectively, given by

$$\begin{aligned} \rho_M(u_\alpha)(\psi) &= (f,\psi) - \Big(\frac{\partial u_\alpha}{\partial t}, \psi\Big) - a(u_\alpha)(\psi) - d(u_\alpha)(\psi) \\ &= -d(u_\alpha)((1-\alpha)\psi), \qquad \text{for any } \psi \in V, \end{aligned} \tag{18}$$

$$\begin{aligned} \overline{\rho}_M(u_\alpha)(\varphi, z_\alpha) &= \mathcal{F}'(u_\alpha)(\varphi) - \Big(\frac{\partial \varphi}{\partial t}, z_\alpha\Big) - a'(u_\alpha)(\varphi, z_\alpha) - d'(u_\alpha)(\varphi, z_\alpha) \\ &= -d'(u_\alpha)(\varphi, (1-\alpha)z_\alpha), \qquad \text{for any } \varphi \in V. \end{aligned} \tag{19}$$

Notice that the residuals $\rho_M(u_\alpha)(\psi)$ and $\overline{\rho}_M(u_\alpha)(\varphi, z_\alpha)$ measure the level to which the adapted solutions (u_α, z_α) fail to satisfy the fine problems (10) and (11), respectively.

The modeling error analysis provided in [3] for steady equations can be generalized to the case of non-stationary problems, thus providing the following result:

Proposition 2.1 *Let us assume that the semilinear forms $a(u_\alpha)(\cdot)$ and $d(u_\alpha)(\cdot)$ and the functional $\mathcal{F}$ are sufficiently differentiable with respect to u_α, for any $\alpha \in L^\infty(Q)$. Then we have*

$$\mathcal{F}(u_1) - \mathcal{F}(u_\alpha) = \underbrace{\rho_M(u_\alpha)(z_\alpha)}_{\text{(I)}} + \underbrace{\frac{1}{2}\big\{\rho_M(u_\alpha)(e_z) + \overline{\rho}_M(u_\alpha)(e_u, z_\alpha)\big\}}_{\text{(II)}} + \underbrace{R(x_\alpha)}_{\text{(III)}}, \quad (20)$$

where the residuals are defined according to (18)-(19)*, $e_u = u_1 - u_\alpha$ and $e_z = z_1 - z_\alpha$ are the primal and dual error, respectively, while*

$$R(x_\alpha) = \frac{1}{2}\int_0^1 L'''(x_\alpha + se)(e,e,e)s(1-s)\,ds, \quad (21)$$

is a remainder term, with $e = (e_u, e_z) = x_1 - x_\alpha$.

Proof. The proof of Theorem 2.1 in [3] can be extended to the unsteady problems (1) and (2). The time derivatives in the definition of the Lagrangians are not troublesome for the proof: the explicit definitions of L and L_α are never involved while only relations (15) and (16) are directly exploited. Thus we easily prove that

$$\mathcal{F}(u_1) - \mathcal{F}(u_\alpha) = -d(u_\alpha)((1-\alpha)z_\alpha) - \frac{1}{2}\left\{d(u_\alpha)((1-\alpha)e_z) + d'(u_\alpha)(e_u, (1-\alpha)z_\alpha)\right\} + R(x_\alpha),$$

i.e. relation (20) after substituting the modeling residuals $\rho_M(u_\alpha)(z_\alpha)$, $\rho_M(u_\alpha)(e_z)$ and $\overline{\rho}_M(u_\alpha)(e_u, z_\alpha)$, according to definitions (18) and (19). □

For the reader's ease we provide the complete proof of result (20) in the Appendix.

Notice that, at this stage, result (20) provides us with an exact expression for the quantity $\mathcal{F}(u_1) - \mathcal{F}(u_\alpha)$. Nevertheless it involves quantities depending on the fine solutions, i.e. the primal and dual errors e_u and e_z. Thus, after neglecting the remainder term $R(x_\alpha)$, error estimates for e_u and e_z, in terms of computable quantities, should be found to make "operative" relation (20). This is the approach followed, for instance, in [17, 19, 20]. Alternatively, to make the right-hand side of (20) useful in practice, one can introduce suitable simplifying assumptions on the problem at hand.
We adopt this second strategy, as in [3]. First we demand for a *stability property* of the functional $L'(x)$, by assuming the existence of a constant $\beta > 0$ such that, for any x_n and $x_m \in X$,

$$\|x_n - x_m\|_X \le \beta\,\|L'(x_n) - L'(x_m)\|_{X'}, \quad (22)$$

$\|\cdot\|_X$ and $\|\cdot\|_{X'}$ denoting the norms associated with the space X and its dual X', respectively. Notice that inequality (22) essentially guarantees the invertibility of $L'(x)$. Moreover we assume that, for any $u \in V$, the semilinear form $d(u)(\cdot)$ and its derivatives are sufficiently small. This last request, combined with (22) and thanks to (5), (15) and the relation $L'_\alpha(x_\alpha)(y) = 0$, for any $y \in X$, guarantees that

$$\|e\|_X = \|x_1 - x_\alpha\|_X \le \beta\,\|L'(x_1) - L'(x_\alpha)\|_{X'} = \beta\,\|\delta L'(x_\alpha)\|_{X'} \le \beta\,C(d)\|x_\alpha\|_X,$$

with $C(d) \ll 1$, i.e. that $e = O(C(d))$. By studying the order of magnitude of the quantities (I), (II) and (III) in (20) in terms of $C(d)$, we get that (I) $= O(C(d))$, while (II) $= O([C(d)]^2)$, and (III) $= O([C(d)]^3)$. These considerations allow us to neglect the terms (II) and (III) in (20), i.e. to estimate the quantity $\mathcal{F}(u_1) - \mathcal{F}(u_\alpha)$ as

$$\mathcal{F}(u_1) - \mathcal{F}(u_\alpha) \simeq \eta_\alpha = \rho_M(u_\alpha)(z_\alpha) = -d(u_\alpha)((1-\alpha)z_\alpha).$$

The quantity η_α is the desired *a posteriori modeling error estimator*, being expressed in terms of computable quantities only. It will suggest where the fine problem rather than the coarse one has to be solved on the computational domain to guarantee the quantity $|\mathcal{F}(u_1) - \mathcal{F}(u_\alpha)|$ below a prescribed tolerance τ. We provide more details about this idea in Section 5.

Remark 2.3 *In Section 5.2 we verify heuristically the considerations made above on the order of magnitude of the terms* (I) *and* (II)*, moving from some particular test cases. This will justify, at least numerically, the requirements made above on the functional $L'(x)$, on the semilinear form $d(u)(\cdot)$ and on its derivatives.*

3 Free-surface flow problems

As pointed out in Section 1, a hierarchy of hydrodynamic models can be derived moving from the 3D Navier-Stokes equations for an incompressible free-surface fluid (see Fig. 1). Now in view of a realistic simulation of the motion of water in a complex hydrodynamic system, we aim to have an operative way to automatically select the regions of the domain where a coarse hydrodynamic model can be solved instead of a finer one. This goal can be achieved, for instance, via a suitable *a posteriori* modeling error analysis such as that one introduced in Section 2. However, as this paper is meant as a first attempt in this direction, in the sequel we limit our analysis to a proper coupling of two-dimensional models belonging to the same family of hydrodynamic models, i.e. to Saint-Venant like equations. As possible next development of this research, a coupling among more heterogeneous hydrodynamic models seems to be reasonable.

Let us consider the hierarchy of free-surface flow models

$$\begin{cases} \dfrac{\partial \mathbf{u}_\alpha}{\partial t} + \alpha\,(\mathbf{u}_\alpha \cdot \nabla)\mathbf{u}_\alpha + g\,\nabla h_\alpha = 0 & \text{with } \ (\mathbf{x},t) \in Q, \\ \dfrac{\partial h_\alpha}{\partial t} + \nabla \cdot (h_\alpha \mathbf{u}_\alpha) = 0 & \text{with } \ (\mathbf{x},t) \in Q, \end{cases} \tag{23}$$

with $\mathbf{u}_\alpha(0) = \mathbf{u}_\alpha^0$, $h_\alpha(0) = h_\alpha^0$ the initial data, where the unknowns $\mathbf{u}_\alpha$ and h_α denote the mean velocity and the total water depth, respectively, while Q and the function α are defined as in Section 2. As α takes on only the values 0 and 1, at each time t_j, the nonlinear convective term in the momentum equation will be "switched-on" only in the regions of Ω where $\alpha(\mathbf{x}, t_j) = 1$, that is, ideally, only where the nonlinear features of the problem at hand significatively influence the target functional $\mathcal{F}$. Moreover, proper boundary conditions will be supplied to the hyperbolic system (23), depending on the

hydrodynamic problem at hand.
According to the notations of the previous section, we will refer to (23) as the *adapted model*, i.e. the system solved in practice.

The choice $\alpha = 1$, for any $(\mathbf{x}, t) \in Q$, provides us with the *fine* model, that is with the Saint-Venant equations [25, 26], written in the non-conservative form:

$$\begin{cases} \dfrac{\partial \mathbf{u}_1}{\partial t} + (\mathbf{u}_1 \cdot \nabla)\mathbf{u}_1 + g\,\nabla h_1 = 0 & \text{with } \ (\mathbf{x}, t) \in Q, \\ \dfrac{\partial h_1}{\partial t} + \nabla \cdot (h_1 \mathbf{u}_1) = 0 & \text{with } \ (\mathbf{x}, t) \in Q, \end{cases} \tag{24}$$

with $\mathbf{u}_1(0) = \mathbf{u}_1^0$, $h_1(0) = h_1^0$ the initial data. Notice that, from a computational viewpoint, system (24) is the most expensive one. The expectation is to never solve the fine model on the whole domain, but only on a reduced portion of Ω. This will be confirmed by the numerical validation in Section 5.2.

On the other hand, if α is identically equal to zero in Q, the adapted model reduces to the *coarse problem*

$$\begin{cases} \dfrac{\partial \mathbf{u}_0}{\partial t} + g\,\nabla h_0 = 0 & \text{with } \ (\mathbf{x}, t) \in Q, \\ \dfrac{\partial h_0}{\partial t} + \nabla \cdot (h_0 \mathbf{u}_0) = 0 & \text{with } \ (\mathbf{x}, t) \in Q. \end{cases} \tag{25}$$

Typically, also problem (25) will be never solved on the whole Ω. Were this the case, it could mean that the hydrodynamics involved in the problem at hand is simpler than what expected a priori, and the coarse model would suffice to reasonably describe the phenomenon.

To summarize, at each time t_j, neither the fine problem (24) nor the coarse one (25) will be solved on the whole Ω. The problem to be discretized will be the adapted model (23), according to the value of $\alpha(\mathbf{x}, t_j)$, for any $(\mathbf{x}, t_j) \in Q$.

3.1 Modeling error estimator for shallow water equations

In view of the derivation of a modeling error estimator for the Saint-Venant equations, let us first fit the free-surface flow models above into the general framework of Section 2. Let us move from the weak form associated with the fine problem (24) and let us sum up the momentum and the continuity equations after multiplication by suitable test functions $\mathbf{v}$ and q, respectively. This leads to the following formulation: find $(\mathbf{u}_1,\, h_1) \in \mathcal{W} = \mathcal{V} \times \mathcal{Z}$ such that, for any $(\mathbf{v},\, q) \in \mathcal{W}$,

$$\Big(\frac{\partial \mathbf{u}_1}{\partial t},\, \mathbf{v}\Big) + \Big(\frac{\partial h_1}{\partial t},\, q\Big) + \big((\mathbf{u}_1 \cdot \nabla)\mathbf{u}_1,\, \mathbf{v}\big) + g\,(\nabla h_1,\, \mathbf{v}) + \big(\nabla \cdot (h_1 \mathbf{u}_1),\, q\big) = 0, \tag{26}$$

with $\mathbf{u}_1(0) = \mathbf{u}_1^0$ and $h_1(0) = h_1^0$. Let us introduce the "global" unknown $U_1 = (\mathbf{u}_1,\, h_1) \in \mathcal{W}$ and test function $\Psi = (\mathbf{v},\, q) \in \mathcal{W}$ to simplify the weak form (26) as: find $U_1 \in \mathcal{W}$ such that

$$\Big(\frac{\partial U_1}{\partial t},\, \Psi\Big) + a(U_1)(\Psi) + d(U_1)(\Psi) = 0, \qquad \text{for any } \Psi \in \mathcal{W}, \tag{27}$$

with $U_1(0) = U_1^0 = (\mathbf{u}_1^0, h_1^0)$ the initial data vector, and where

$$\Big(\frac{\partial U_1}{\partial t},\, \Psi\Big) = \Big(\frac{\partial \mathbf{u}_1}{\partial t},\, \mathbf{v}\Big) + \Big(\frac{\partial h_1}{\partial t},\, q\Big) \tag{28}$$

while

$$a(U_1)(\Psi) = g\ (\nabla h_1,\, \mathbf{v}) + \big(\nabla \cdot (h_1 \mathbf{u}_1),\, q\big) \quad \text{and} \quad d(U_1)(\Psi) = \big((\mathbf{u}_1 \cdot \nabla)\mathbf{u}_1,\, \mathbf{v}\big) \tag{29}$$

are semilinear forms, linear with respect to Ψ but nonlinear in U_1. Notice that, in this case, the forcing term in (2) is identically equal to zero.

Remark 3.1 *The spaces $\mathcal{V}$ and $\mathcal{Z}$ are chosen according to the boundary conditions associated with system* (24)*, i.e. according to the test case under examination. At this stage, we have considered the general problem* (24) *without choosing specific boundary conditions. Thus we can only state that $\mathcal{V}$ and $\mathcal{Z}$ are suitable subspaces of $H^1(\Omega) \times H^1(\Omega)$ and $H^1(\Omega)$, respectively.*

Now let $\mathcal{F}$ be the goal functional we are interested in. Following the constrained minimization procedure of Section 2, we first introduce the *fine* Lagrangian

$$L(\widetilde{x}_1) = \mathcal{F}(U_1) - a(U_1)(Z_1) - d(U_1)(Z_1) - \Big(\frac{\partial U_1}{\partial t},\, Z_1\Big), \tag{30}$$

with $\widetilde{x}_1 = (U_1, Z_1) \in \widetilde{X} = \mathcal{W} \times \mathcal{W}$, and where $Z_1 = (\mathbf{w}_1, \kappa_1) \in \mathcal{W}$ is the vector of the Lagrange multipliers (or influence functions) associated with the functional $\mathcal{F}$. Thus, when looking for the stationary point $\widetilde{x}_1$ of the Lagrangian L in (30), we are led to solving the fine primal problem (27) together with the corresponding dual one: find $Z_1 \in \mathcal{W}$ such that

$$\Big(\frac{\partial \Phi}{\partial t},\, Z_1\Big) + a'(U_1)(\Phi, Z_1) + d'(U_1)(\Phi, Z_1) = \mathcal{F}'(U_1)(\Phi), \qquad \text{for any } \Phi \in \mathcal{W},$$

with $Z_1(T) = Z_1^T = (\mathbf{w}_1^T, \kappa_1^T)$ the final data vector, and $\Phi = (\boldsymbol{\varphi}, \vartheta)$ the test functions pair.
According to the Gâteaux derivative definition, we have that

$$a'(U_1)(\Phi, Z_1) = g(\nabla \vartheta, \mathbf{w}_1) + \big(\nabla \cdot (h_1 \boldsymbol{\varphi}), \kappa_1\big) + \big(\nabla \cdot (\vartheta \mathbf{u}_1), \kappa_1\big), \tag{31}$$

$$d'(U_1)(\Phi, Z_1) = \big((\mathbf{u}_1 \cdot \nabla)\boldsymbol{\varphi}, \mathbf{w}_1\big) + \big((\boldsymbol{\varphi} \cdot \nabla)\mathbf{u}_1, \mathbf{w}_1\big). \tag{32}$$

Moreover, notice that the components $\mathbf{w}_1$ and κ_1 of the dual solution Z_1 may be defined as the dual mean velocity and the dual total water depth, respectively.

Now, let us consider the adapted model (23). By repeating an analogous procedure, we introduce the adapted weak form: find $U_\alpha = (\mathbf{u}_\alpha,\, h_\alpha) \in \mathcal{W}$ such that

$$\Big(\frac{\partial U_\alpha}{\partial t},\, \Psi\Big) + a(U_\alpha)(\Psi) + d(U_\alpha)(\alpha\Psi) = 0, \qquad \text{for any } \Psi = (\mathbf{v},\, q) \in \mathcal{W}, \tag{33}$$

with $U_\alpha(0) = U_\alpha^0 = (\mathbf{u}_\alpha^0, h_\alpha^0)$ the initial data vector and where the scalar product $\Big(\dfrac{\partial U_\alpha}{\partial t},\, \Psi\Big)$ and the semilinear forms $a(U_\alpha)(\cdot)$ and $d(U_\alpha)(\cdot)$ are defined according to (28) and (29), respectively. Via a minimization procedure, we are led to looking for the critical point $\widetilde{x}_\alpha = (U_\alpha, Z_\alpha) \in \widetilde{X}$ of the *adapted* Lagrangian

$$L_\alpha(\widetilde{x}_\alpha) = \mathcal{F}(U_\alpha) - a(U_\alpha)(Z_\alpha) - d(U_\alpha)(\alpha Z_\alpha) - \Big(\frac{\partial U_\alpha}{\partial t},\, Z_\alpha\Big),$$

i.e., to finding the solution $U_\alpha \in \mathcal{W}$ of the adapted primal problem (33) together with the solution $Z_\alpha = (\mathbf{w}_\alpha, \kappa_\alpha) \in \mathcal{W}$ of the associated dual problem: find $Z_\alpha \in \mathcal{W}$ such that

$$\Big(\frac{\partial \Phi}{\partial t},\, Z_\alpha\Big) + a'(U_\alpha)(\Phi, Z_\alpha) + d'(U_\alpha)(\Phi, \alpha Z_\alpha) = \mathcal{F}'(U_\alpha)(\Phi), \qquad \text{for any } \Phi \in \mathcal{W}, \quad (34)$$

with $Z_\alpha(T) = Z_\alpha^T = (\mathbf{w}_\alpha^T, \kappa_\alpha^T)$, $\Phi = (\boldsymbol{\varphi}, \vartheta)$, and where the scalar product $\Big(\dfrac{\partial \Phi}{\partial t},\, Z_\alpha\Big)$ and the semilinear forms $a'(U_\alpha)(\Phi, Z_\alpha)$ and $d'(U_\alpha)(\Phi, \alpha Z_\alpha)$ are defined according to (28), (31) and (32), respectively.

We are now in a position to state the result corresponding to Proposition 2.1 for the free-surface flow models (23). With this aim, let us introduce the modeling residuals involved in (20):

$$\begin{aligned}
\rho_M(U_\alpha)(Z_\alpha) &= -d(U_\alpha)\big((1-\alpha)Z_\alpha\big) = -\big((\mathbf{u}_\alpha \cdot \nabla)\mathbf{u}_\alpha,\, (1-\alpha)\mathbf{w}_\alpha\big), \\
\rho_M(U_\alpha)(E_Z) &= -d(U_\alpha)\big((1-\alpha)E_Z\big) = -\big((\mathbf{u}_\alpha \cdot \nabla)\mathbf{u}_\alpha,\, (1-\alpha)(\mathbf{w}_1 - \mathbf{w}_\alpha)\big), \\
\overline{\rho}_M(U_\alpha)(E_U, Z_\alpha) &= -d'(U_\alpha)\big(E_U, (1-\alpha)Z_\alpha\big) \qquad (35) \\
&= -\big((\mathbf{u}_\alpha \cdot \nabla)(\mathbf{u}_1 - \mathbf{u}_\alpha), (1-\alpha)\mathbf{w}_\alpha\big) - \big(\big((\mathbf{u}_1 - \mathbf{u}_\alpha) \cdot \nabla\big)\mathbf{u}_\alpha, (1-\alpha)\mathbf{w}_\alpha\big),
\end{aligned}$$

where $E_U = (\mathbf{u}_1 - \mathbf{u}_\alpha, h_1 - h_\alpha)$ and $E_Z = (\mathbf{w}_1 - \mathbf{w}_\alpha, \kappa_1 - \kappa_\alpha)$ are the primal and dual error, respectively.

Proposition 3.1 *If the semilinear forms $a(U_\alpha)(\cdot)$ and $d(U_\alpha)(\cdot)$ defined in* (29) *and the functional $\mathcal{F}$ are sufficiently differentiable with respect to U_α, for any $\alpha \in L^\infty(Q)$, then it holds that*

$$\mathcal{F}(U_1) - \mathcal{F}(U_\alpha) = \underbrace{\rho_M(U_\alpha)(Z_\alpha)}_{\text{(I)}} + \underbrace{\frac{1}{2}\big\{\rho_M(U_\alpha)(E_Z) \,+\, \overline{\rho}_M(U_\alpha)(E_U, Z_\alpha)\big\}}_{\text{(II)}} + \underbrace{R(\widetilde{x}_\alpha)}_{\text{(III)}}, \quad (36)$$

the residuals $\rho_M(U_\alpha)(Z_\alpha)$, $\rho_M(U_\alpha)(E_Z)$ and $\overline{\rho}_M(U_\alpha)(E_U, Z_\alpha)$ and the remainder term $R(\widetilde{x}_\alpha)$ being defined according to (35) *and* (21)*, respectively.*

To make result (36) practical from a computational viewpoint, we make the same simplifying hypotheses of stability on $L'(x)$ and of regularity on $d(U)(\cdot)$ and its derivatives as introduced in Section 2, for any $x \in \widetilde{X}$ and for any $U \in \mathcal{W}$. Thus, the following modeling error estimator for the goal quantity $\mathcal{F}(U_1) - \mathcal{F}(U_\alpha)$ is obtained:

$$\mathcal{F}(U_1) - \mathcal{F}(U_\alpha) \simeq \eta_\alpha = \rho_M(U_\alpha)(Z_\alpha) = -\big((\mathbf{u}_\alpha \cdot \nabla)\mathbf{u}_\alpha,\, (1-\alpha)\mathbf{w}_\alpha\big). \qquad (37)$$

Remark 3.2 *Notice that, at this stage, we are interested in the modeling error control only, i.e. we are assuming to replace in (37) the quantities* $\mathbf{u}_\alpha$ *and* $\mathbf{w}_\alpha$ *with sufficiently accurate approximations* $\mathbf{u}_{h,\alpha}$ *and* $\mathbf{w}_{h,\alpha}$*, respectively (we refer to Section 5.2 for some further remarks). An example of analysis taking into account both the discretization and the modeling error is provided in [3].*

Remark 3.3 *As pointed out in Section 2 for the general unsteady case, to get useful information from (36), we could also find a bound for the errors* E_U *and* E_Z *in terms of the adapted quantities* U_α *and* Z_α *(see [17, 19, 20]). This alternative approach would avoid us to make the stability and regularity assumptions above on* $L'(x)$ *and on* $d(U)(\cdot)$ *and its derivatives. However, this task is not trivial for the shallow water equations, unless one probably moves from a conservative and viscous formulation of the shallow water system.*

4 The discretization scheme

According to the theory developed in the previous sections, the problems to be approximate at each time t_j are the adapted primal and dual ones. They both are discretized via a space-time finite element scheme. In more detail we use the cG(1)dG(0) method, by choosing functions continuous and piecewise linear in space, discontinuous and piecewise constant in time [11, 5].
With this aim, we move from the general cG(1)dG(r) discretization of the equations (33) and (34), with $r \geq 0$. Let us introduce a partition of the time interval $(0, T]$, $0 = t_0 < t_1 < \ldots < t_n = T$ into subintervals $I_i = (t_{i-1}, t_i]$ of length $k_i = t_i - t_{i-1}$, for $i = 1, \ldots, n$. The space-time domain Q turns out to be subdivided into n space-time slabs $S_i = \Omega \times I_i$. The discontinuity of the time discretization allows us to endow each slab S_i with a different mesh and justifies the definition of jump of a function v at time t_j, for $j = 1, \ldots, n-1$, given by

$$[v]_j = v^{j,+} - v^{j,-}, \qquad \text{where} \qquad v^{j,\pm} = \lim_{s \to 0} v(t_j \pm s).$$

Let us introduce the space-time finite element space

$$V_{h,1}^{k,r} = \Big\{ v \in L^\infty(0, T, C^0(\overline{\Omega})) : \; v(\mathbf{x}, t)\big|_{I_i} = \sum_{j=0}^{r} v_j^i(\mathbf{x})\, t^j, \; v_j^i \in V_h^i \Big\}, \tag{38}$$

for $r \geq 0$. The space V_h^i in (38) is the standard space of continuous piecewise linear finite elements, associated with the mesh on S_i and suitably accounting for the boundary conditions assigned on $\partial\Omega$.
Thus the cG(1)dG(r) discrete form of the adapted primal problem (33) reads as: find

$U_{h,\alpha} = (\mathbf{u}_{h,\alpha}, h_{h,\alpha}) \in V_{h,1}^{k,r}$ such that, for any $\Psi_h = (\mathbf{v}_h, q_h) \in V_{h,1}^{k,r}$,

$$\begin{aligned}
&\int_0^T \int_\Omega \Big\{ \frac{\partial \mathbf{u}_{h,\alpha}}{\partial t} \cdot \mathbf{v}_h + \frac{\partial h_{h,\alpha}}{\partial t}\, q_h + g\, \nabla h_{h,\alpha} \cdot \mathbf{v}_h + \nabla \cdot (h_{h,\alpha} \mathbf{u}_{h,\alpha})\, q_h \\
&+ \alpha\, (\mathbf{u}_{h,\alpha} \cdot \nabla) \mathbf{u}_{h,\alpha} \cdot \mathbf{v}_h \Big\}\, d\Omega\, dt + \sum_{i=1}^{n-1} \big([\mathbf{u}_{h,\alpha}]_i, \mathbf{v}_h^{i,+} \big)_\Omega + \sum_{i=1}^{n-1} \big([h_{h,\alpha}]_i, q_h^{i,+} \big)_\Omega \\
&+ \big(\mathbf{u}_{h,\alpha}^{0,+}, \mathbf{v}_h^{0,+} \big)_\Omega + \big(h_{h,\alpha}^{0,+}, q_h^{0,+} \big)_\Omega = \big(\mathbf{u}_\alpha^0, \mathbf{v}_h^{0,+} \big)_\Omega + \big(h_\alpha^0, q_h^{0,+} \big)_\Omega,
\end{aligned} \tag{39}$$

$(\cdot,\cdot)_\Omega$ being the standard $L^2(\Omega)$-scalar product. For the value $i = 0$, we have set $[\mathbf{u}_{h,\alpha}]_0 = \mathbf{u}_{h,\alpha}^{0,+} - \mathbf{u}_\alpha^0$ and $[h_{h,\alpha}]_0 = h_{h,\alpha}^{0,+} - h_\alpha^0$, where $\mathbf{u}_\alpha^0$ and h_α^0 are the initial data associated with (23). Likewise, the adapted dual problem (34) is discretized as: find $Z_{h,\alpha} = (\mathbf{w}_{h,\alpha}, \kappa_{h,\alpha}) \in V_{h,1}^{k,r}$ such that, for any $\Phi_h = (\boldsymbol{\varphi}_h, \vartheta_h) \in V_{h,1}^{k,r}$,

$$\begin{aligned}
&\int_T^0 \int_\Omega \Big\{ \frac{\partial \boldsymbol{\varphi}_h}{\partial t} \cdot \mathbf{w}_{h,\alpha} + \frac{\partial \vartheta_h}{\partial t}\, \kappa_{h,\alpha} + g\, \nabla \vartheta_h \cdot \mathbf{w}_{h,\alpha} + \nabla \cdot (h_{h,\alpha}\, \boldsymbol{\varphi}_h)\, \kappa_{h,\alpha} + \nabla \cdot (\vartheta_h\, \mathbf{u}_{h,\alpha})\, \kappa_{h,\alpha} \\
&+ \alpha\, (\mathbf{u}_{h,\alpha} \cdot \nabla) \boldsymbol{\varphi}_h \cdot \mathbf{w}_{h,\alpha} + \alpha\, (\boldsymbol{\varphi}_h \cdot \nabla) \mathbf{u}_{h,\alpha} \cdot \mathbf{w}_{h,\alpha} \Big\}\, d\Omega\, dt - \sum_{i=1}^{n-1} \big([\mathbf{w}_{h,\alpha}]_i, \boldsymbol{\varphi}_h^{i,-} \big)_\Omega \\
&- \sum_{i=1}^{n-1} \big([\kappa_{h,\alpha}]_i, \vartheta_h^{i,-} \big)_\Omega + \big(\mathbf{w}_{h,\alpha}^{n,-}, \boldsymbol{\varphi}_h^{n,-} \big)_\Omega + \big(\kappa_{h,\alpha}^{n,-}, \vartheta_h^{n,-} \big)_\Omega = \mathcal{F}'(U_{h,\alpha})(\Phi_h) \\
&+ \big(\mathbf{w}_\alpha^T, \boldsymbol{\varphi}_h^{n,-} \big)_\Omega + \big(\kappa_\alpha^T, \vartheta_h^{n,-} \big)_\Omega.
\end{aligned} \tag{40}$$

For the value $i = n$, we have set $\big([\mathbf{w}_{h,\alpha}]_n, \boldsymbol{\varphi}_h^{n,-} \big)_\Omega = (\mathbf{w}_\alpha^T - \mathbf{w}_{h,\alpha}^{n,-}, \boldsymbol{\varphi}_h^{n,-})$ and $\big([\kappa_{h,\alpha}]_n, \vartheta_h^{n,-} \big)_\Omega = (\kappa_\alpha^T - \kappa_{h,\alpha}^{n,-}, \vartheta_h^{n,-})$, with $\mathbf{w}_\alpha^T$ and κ_α^T the final data completing (34).
As we aim to use functions piecewise constant in time (namely, an implicit Euler scheme for the time discretization), we set $r = 0$ in (38). The time derivatives in (39) and (40) are thus identically equal to zero. Moreover the discontinuous nature of the time discretization scheme allows us to decouple the global systems (39) and (40), and rewrite them as a time-stepping scheme, i.e.

$$\begin{aligned}
&\int_{t_{i-1}}^{t_i} \int_\Omega \Big\{ g\, \nabla h_{h,\alpha} \cdot \mathbf{v}_h + \nabla \cdot (h_{h,\alpha} \mathbf{u}_{h,\alpha})\, q_h + \alpha\, (\mathbf{u}_{h,\alpha} \cdot \nabla) \mathbf{u}_{h,\alpha} \cdot \mathbf{v}_h \Big\}\, d\Omega\, dt \\
&\qquad + \big([\mathbf{u}_{h,\alpha}]_{i-1}, \mathbf{v}_h^{i-1,+} \big)_\Omega + \big([h_{h,\alpha}]_{i-1}, q_h^{i-1,+} \big)_\Omega = 0,
\end{aligned} \tag{41}$$

and

$$\begin{aligned}
&\int_{t_i}^{t_{i-1}} \int_\Omega \Big\{ g\, \nabla \vartheta_h \cdot \mathbf{w}_{h,\alpha} + \nabla \cdot (h_{h,\alpha}\, \boldsymbol{\varphi}_h)\, \kappa_{h,\alpha} + \nabla \cdot (\vartheta_h\, \mathbf{u}_{h,\alpha})\, \kappa_{h,\alpha} + \alpha\, (\mathbf{u}_{h,\alpha} \cdot \nabla) \boldsymbol{\varphi}_h \cdot \mathbf{w}_{h,\alpha} \\
&+ \alpha\, (\boldsymbol{\varphi}_h \cdot \nabla) \mathbf{u}_{h,\alpha} \cdot \mathbf{w}_{h,\alpha} \Big\}\, d\Omega\, dt - \big([\mathbf{w}_{h,\alpha}]_i, \boldsymbol{\varphi}_h^{i,-} \big)_\Omega - \big([\kappa_{h,\alpha}]_i, \vartheta_h^{i,-} \big)_\Omega = \mathcal{F}'(U_{h,\alpha})(\Phi_h),
\end{aligned} \tag{42}$$

respectively, for $i = 1, \ldots, n$.

It is well-known that the resolution of the coupled discrete problems (41) and (42) is not a trivial matter, essentially due to the reverse time scales characterizing the dual framework. This could make the computational cost of the whole space-time discretization extremely burdensome, especially for a large time interval and when a small time step is required to guarantee the convergence of the discretization scheme.
Ideally, in view of an adaptive procedure based on the error estimator η_α in (37), one first solves the coarse primal problem and the coarse dual problem on the intervals $(t_0, T]$ and $(T, t_0]$, respectively, to get the starting solutions (see Section 5.1 for the details). Then, to get the value predicted by η_α for the goal quantity $\mathcal{F}(U_1) - \mathcal{F}(U_\alpha)$, two new advancings in time, one forward and the other backward, are necessary to find suitable approximations for the quantities U_α and Z_α in (37). Overall, the whole time interval has to be spanned four times, twice forward and twice backward.

Remark 4.1 *To reduce the computational cost of the rigorous "primal-dual" procedure described above, different heuristic strategies can be adopted. A first approach we tested moves from the assumption that the goal output functional $\mathcal{F}$ is a global "space-time" functional, that can be written as*

$$\mathcal{F}(\cdot) = \int_0^T \int_\Omega g(\cdot)\, d\Omega\, dt, \tag{43}$$

with g a positive function. In such a case, a "slab-wise" procedure can be adopted. In more detail, both the primal and the dual problems are solved, forward and backward, respectively, for each space-time slab S_i, for $i = 1, \ldots, n$. The discontinuous nature of the adopted time discretization together with the choice made in (43) for the goal functional $\mathcal{F}$ justify such an approach. However, by comparing the numerical results provided by this approach with the corresponding ones yielded by the rigorous "primal-dual" procedure, it is found that the minimum for $\mathcal{F}$ from the "slab-wise" procedure generally is an overestimation of the minimum detected by the rigorous approach.
A second more reliable strategy is proposed and validated in Section 5.2.

5 Numerical assessment

The aim of this section is twofold. Moving from the modeling error estimator (37), we first sketch the algorithm used to decide which model of the hierarchy (23) has to be solved at each time and on each mesh element K, to guarantee a prescribed tolerance τ on the goal quantity $|\mathcal{F}(U_1) - \mathcal{F}(U_\alpha)|$. Then we validate this algorithm on some numerical test cases.

5.1 The adaptive procedure

Let us introduce a fixed space-time partition of the computational domain Q consisting of N_h elements and N_t uniform time intervals. To start the model adaption procedure we

need a reference primal and dual solution. With this aim, we first discretize the coarse primal problem (25) on $(0,T]$, together with the corresponding dual problem (equation (34) with $\alpha = 0$) on $(T,0]$ and compute $\eta_\alpha = \eta_0$. Now we are in a position to apply the adaptive procedure below:

1) via a suitable *localization* procedure, the estimator η_α is evaluated on each triangle K and on each time interval I_i, thus yielding the local positive modeling error estimator $\eta^i_{\alpha,K} = \eta_\alpha|_{K\times I_i}$;

2) then:

   a) if $\eta^i_{\alpha,K} > \dfrac{\tau}{N_h N_t}$, then $\alpha|_{K\times I_i} = 1$, i.e. the fine model (24) is associated with the element K of the space-time slab S_i;

   b) if $\eta^i_{\alpha,K} \leq \dfrac{\tau}{N_h N_t}$, then $\alpha|_{K\times I_i} = 0$, i.e. the coarse model (25) is discretized on the triangle K of the space-time slab S_i;

3) the adapted primal and dual problems (33) and (34) are thus discretized, the corresponding function α being identified at the points 2)-a) and 2)-b);

4) the quantity η_α is finally evaluated.

Notice that a sub-iteration on the points 2)-a) and 2)-b) will be likely required to guarantee the global quantity $|\mathcal{F}(U_1) - \mathcal{F}(U_\alpha)|$ to be really under the prescribed tolerance τ, in spite of the localization procedure. Moreover the check at the points 2)-a) and 2)-b) entails a space-time equidistribution criterion of the modeling error on the elements of the mesh.

Remark 5.1 *The localization procedure used at point 1) is similar to the one adopted in [3].*

Remark 5.2 *Concerning the choice of the computational grid, the idea is to use a mesh fine enough so that the discretization error be at least an order of magnitude less than the tolerance τ demanded on the modeling error. Some further considerations related to this choice will be made in the wave overpassing a cylinder test case.*

The adaptive approach described above turns out to be a reliable procedure in spite of its simplicity. This is confirmed by the numerical results in the next section.

5.2 The numerical test cases

A numerical validation of the adaptive procedure in Section 5.1 is provided here. In more detail three different two-dimensional hydrodynamic configurations are considered. The first one deals with the simulation of the motion of a wave in a closed basin. In the second test case the evolution of a solitary wave moving along a straight channel with an obstacle is analyzed. Finally, in the last test case we simulate the motion of a solitary wave along a river bifurcation.

5.2.1 The Gaussian hill test case

A well-known example of the Gaussian hill phenomenon is provided by the evolution of the water surface when, for instance, a stone is thrown into the water at rest.
Let the computational domain $\Omega = (-20, 20) \times (-20, 20) \subset \mathbb{R}^2$ be a closed squared basin with a side of $40m$. The reference water level is chosen equal to $5m$ and the bottom is assumed flat. The adapted model (23) is completed with suitable initial and boundary conditions. In more detail, at the initial time $t_0 = 0$, the profile of elevation

$$h_\alpha(x, y, 0) = e^{-0.25(x^2+y^2)} \tag{44}$$

is assumed. Equation (44) describes the Gaussian hill centered at $(0, 0)m$ and with height equal to $1m$. In absence of the Coriolis force, the Gaussian hill breaks and gives rise to a circular wave propagating from the point $(0, 0)m$ towards the boundary of the domain. Then, as the basin is closed, the wave is reflected backward to the center of the domain. Concerning the boundary conditions, no-slip conditions are assigned for the velocity $\mathbf{u}_\alpha$ on the whole boundary $\partial\Omega$ of the domain, namely we impose $\mathbf{u}_\alpha \cdot \mathbf{n} = 0$, $\mathbf{n}$ being the unit outward normal vector to the boundary $\partial\Omega$.
To discretize system (23) and the corresponding dual problem with the cG(1)dG(0) scheme of Section 4, a quasi-uniform mesh of $N_h = 21248$ elements is employed, while the time step Δt is chosen equal to $0.1s$, the final time being $T = 16s$.
Finally we identify the goal functional $\mathcal{F}$ with the quantity

$$\mathcal{F}(U_1) = \mathcal{F}_{GH}^{kin,\,\Omega}(U_1) = \int_0^T \int_\Omega |U_1|^2 \, d\Omega \, dt, \tag{45}$$

representing the *kinetic energy* of the fluid. A tolerance $\tau = 10^{-3}$ is required on the value $\mathcal{F}_{GH}^{kin,\,\Omega}(U_\alpha)$ approximating the goal quantity (45).

Let us analyze the numerical results. Figure 3 shows the distribution of the areas corresponding to the fine model (dark zones) and to the coarse one (light zones) at six different times. In more detail, at each time t_j the adapted free-surface model (23) is solved on the whole domain Ω, the piecewise constant function α being identically equal to 1 in correspondence of the dark areas and equal to 0 in the light zones. The subregions that influence most the kinetic energy of the fluid are associated with the fine model. In particular, both the initial and the reflected wave are detected by the error estimator.

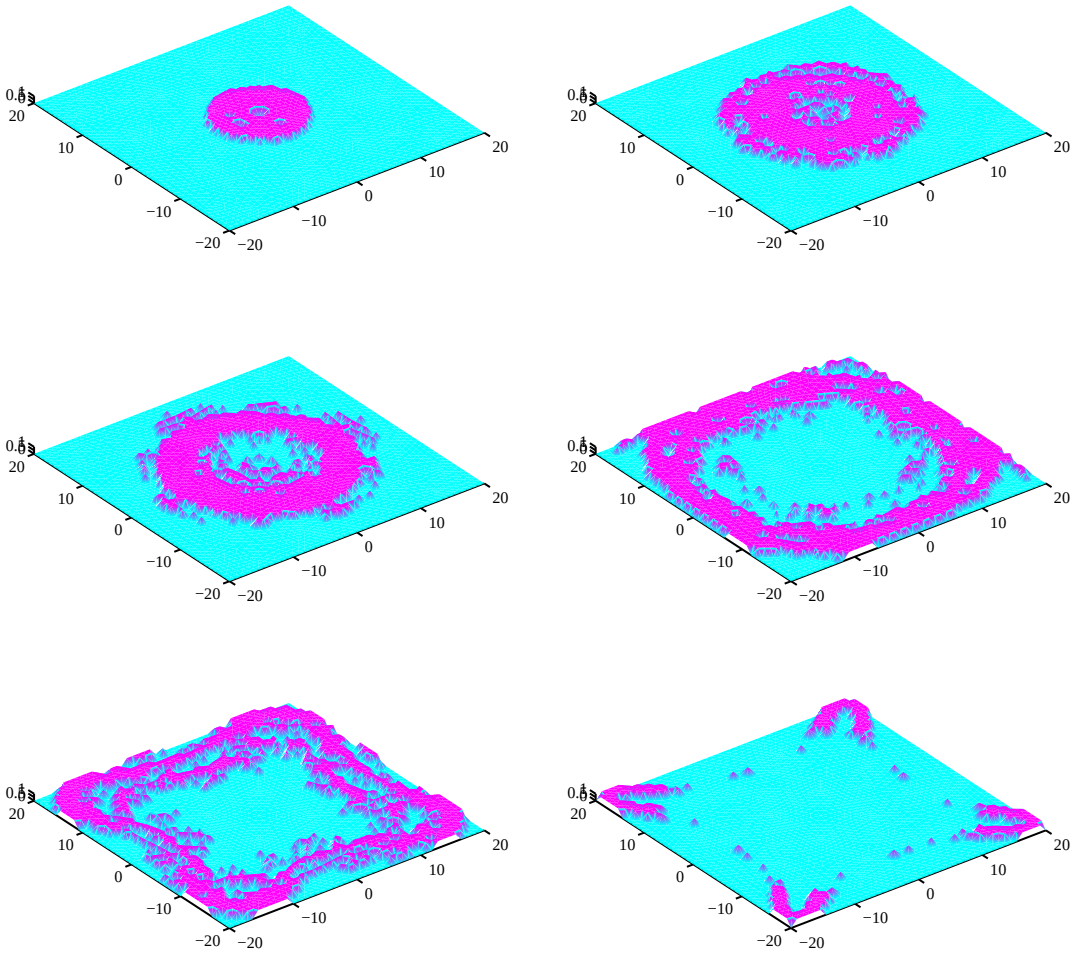

Figure 3: Distribution of the areas associated with the fine model (dark zones) and with the coarse model (light zones) for the Gaussian hill test case. Left-right, top-bottom: $t_j = 1s$, $3s$, $4s$, $7s$, $9s$ and $10s$

Notice that the not perfect symmetry characterizing the distribution of the fine and of the coarse areas at the times $t_j = 4s$ and $t_j = 7s$ is likely due to the unstructured computational grid. Moreover we remark that the number of the mesh elements where the fine model is discretized is, at each time, a reduced portion of the total number of triangles, being at most 35% of the total number of elements. Figure 4 confirms such a feature: the maximum number of triangles associated with the fine model is reached at $t_j = 9s$, namely at the beginning of the whole reflection phase of the wave.

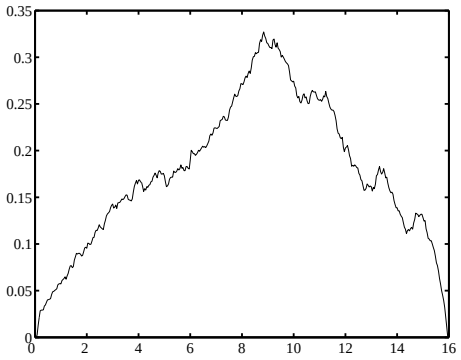

Figure 4: Time evolution of the percentage of mesh triangles associated with the fine model for the Gaussian hill test case

In Fig. 5 the estimates provided by η_α for the quantity $|\mathcal{F}_{GH}^{kin,\Omega}(U_1) - \mathcal{F}_{GH}^{kin,\Omega}(U_\alpha)|$ are represented in correspondence with the times $t_j = 4s$, $7s$ and $10s$. The accuracy required on the approximation $\mathcal{F}_{GH}^{kin,\Omega}(U_\alpha)$ is guaranteed, the values in Fig. 5 being all approximatively within the demanded tolerance $\tau = 10^{-3}$. Moreover, a comparison between the plots of Figures 3 and 5 corresponding to the same times, shows that, as expected, the largest values of η_α are associated with the areas of the domain where the fine model is solved.

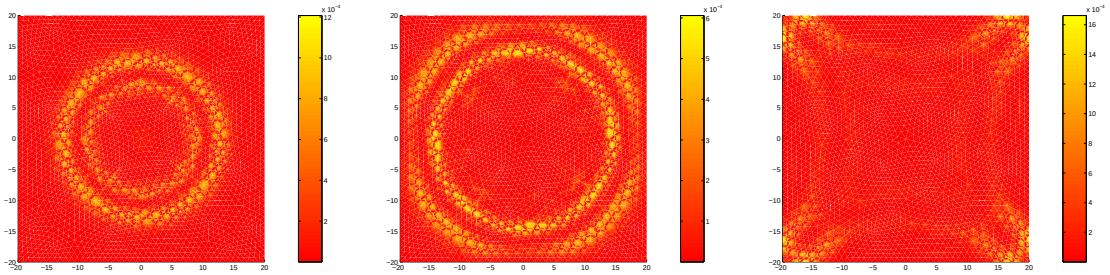

Figure 5: Values provided by η_α for the quantity $|\mathcal{F}_{GH}^{kin,\Omega}(U_1) - \mathcal{F}_{GH}^{kin,\Omega}(U_\alpha)|$ at the times $t_j = 4s$ (left), $t_j = 7s$ (middle) and $t_j = 10s$ (right)

Due to the academic nature of this test case, we have used it to make some further assessment on the adopted numerical procedure. In more detail, we have first analyzed the sensitivity of the results with respect to the time step Δt. We have evaluated the error estimator η_α for three different choices of the tolerance τ and two different values of Δt. The corresponding results are summarized in Table 1.
Except for the choice $\tau = 10^{-2}$ and $\Delta t = 0.1s$, all the values tabulated for η_α are largely below the prescribed tolerance. In particular, for the smaller time step, an additional order of magnitude is gained with respect to the demanded accuracy. However, notice that a smaller time step necessarily involves an increase of the computational cost!

On this test case, we have also validated a numerical strategy for the evaluation of the estimator η_α, alternative to the rigorous "primal-dual" approach of Section 4 and

τ	$\Delta t = 0.1$	$\Delta t = 0.05$
10^{-2}	$1.0065 \cdot 10^{-2}$	$5.2508 \cdot 10^{-4}$
10^{-3}	$3.0474 \cdot 10^{-4}$	$2.8198 \cdot 10^{-5}$
10^{-4}	$4.0255 \cdot 10^{-5}$	$2.6961 \cdot 10^{-6}$

Table 1: Sensitivity of the error estimator η_α with respect to the time step Δt for the Gaussian hill test case

to the "slab-wise" procedure of Remark 4.1. In more detail, the quantity η_α in (37) is replaced by the new one $\eta_\alpha = \rho_M(U_\alpha)(Z_0) = -\big((\mathbf{u}_\alpha \cdot \nabla)\mathbf{u}_\alpha, (1-\alpha)\mathbf{w}_0\big)$. From a computational viewpoint this choice is reasonable, the time interval being spanned now only three times. From a theoretical point of view, this strategy can be justified as in a *dual-weighted residual* approach where the quantitative information is provided by the primal problem, the dual problem being responsible essentially of weighting how the error propagates.

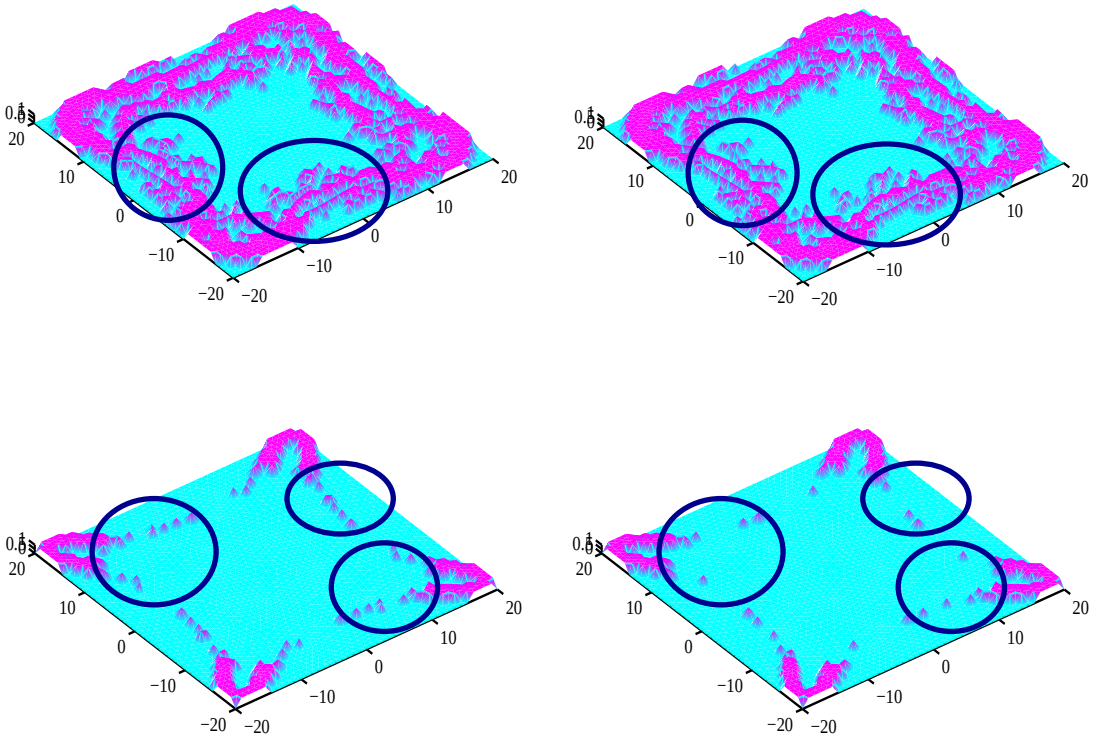

Figure 6: Distribution of the areas associated with the fine model (dark zones) and with the coarse model (light zones) provided by the rigorous "primal-dual' approach (on the right) and by the simplified one (on the left) for the Gaussian hill test case. Top-bottom: $t_j = 9s$ and $10s$

Figure 6 compares the distribution of the fine and of the coarse areas provided by the rigorous approach and by the simplified one at times $t_j = 9s$ and $t_j = 10s$. The zones which differ more significantly are highlighted by the ellipses. However, notice that the results provided by the two approaches almost coincide.

5.2.2 The channel with an obstacle test case

Let us analyze the motion of a solitary wave along a straight channel with an obstacle. We identify the computational domain $\Omega \subset \mathbb{R}^2$ with a channel $100m$ long and $20m$ wide, characterized by a cylinder centered at $(x, y) = (30, 10)m$ and with a radius $r = 4m$. The reference water level is chosen equal to $5m$ and the bottom is assumed flat. The initial conditions associated with the adapted model (23) are the following ones:

$$\begin{aligned} u_\alpha(x,\, y,\, 0) = \sqrt{11.76}\, \frac{0.2\,\mathrm{sech}^2(\sqrt{0.15}(x-10))}{5 + 0.2\,\mathrm{sech}^2(\sqrt{0.15}(x-10))}, \qquad v_\alpha(x,\, y,\, 0) = 0, \\ h_\alpha(x,\, y,\, 0) = 0.2\,\mathrm{sech}^2(\sqrt{0.15}(x-10)) + 5, \end{aligned} \tag{46}$$

u_α and v_α being the x- and y-component of the mean velocity $\mathbf{u}_\alpha$, respectively. Equations (46) describe the velocity and the elevation profile characterizing a so-called solitary wave, namely a wave traveling with the same velocity and without any shape distortion if any perturbation does not occur [26], as an obstacle. Thus, when the solitary wave overpasses the cylinder, a reflected wave, moving backward with respect to the direction of the solitary wave, is generated.
Non-reflecting boundary conditions are assigned at the inflow and at the outflow of the domain, while no-slip conditions (i.e. $\mathbf{u}_\alpha \cdot \mathbf{n} = 0$) are associated with the horizontal sides of Ω.
The cG(1)dG(0) scheme of Section 4 is used to discretize system (23) moving from the quasi-uniform grid of $N_h = 2304$ triangles in Fig. 7 (on the left), and by choosing a time step $\Delta t = 0.1s$, with $T = 16s$ the final time.

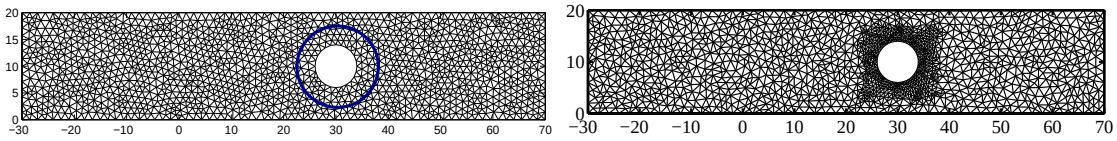

Figure 7: The channel with an obstacle test case: the first computational grid, where the control area γ is highlighted (on the left); the second computational mesh with the local refinement around the cylinder (on the right)

Concerning the goal functional $\mathcal{F}$, we first aim to control the quantity

$$\mathcal{F}(U_1) = \mathcal{F}_{Cyl}^{kin,\,\gamma}(U_1) = \int_0^T \int_\gamma |U_1|^2 \, d\Omega \, dt,$$

that is the kinetic energy of the fluid in the ring region $\gamma \subset \Omega$, of thickness $4m$, around the obstacle (see the highlighted area in Fig. 7, on the left). The tolerance is set to $\tau = 10^{-3}$.
The distribution of the fine and of the coarse areas selected by the error estimator (37) at times $t_j = 6s$, $7s$, $8s$, $9s$, $10s$ and $14s$ is provided in Fig. 8. Now, as we are controlling the goal quantity around the cylinder, it is reasonable for the fine model to be associated with the zones surrounding the obstacle only. It's quite likely that the solitary wave provides information to the target functional $\mathcal{F}$ during the interaction of the wave with the cylinder, when we expect the fine model to become "active".

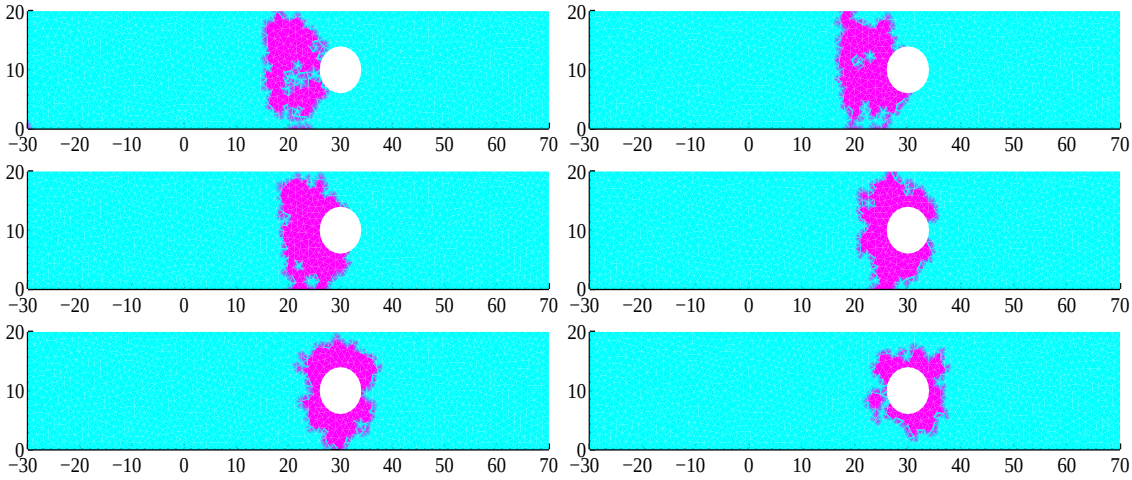

Figure 8: Distribution of the areas associated with the fine model (dark zones) and with the coarse model (light zones) for the channel with an obstacle test case and for the choice $\mathcal{F} = \mathcal{F}_{Cyl}^{kin,\gamma}$. Left-right, top-bottom: $t_j = 6s$, $7s$, $8s$, $9s$, $10s$ and $14s$

To stress the dependence of the "area-to-model" correspondence on the selected goal functional, we show in Fig. 9 the distribution of the regions where the fine and the coarse models are solved for two different functionals $\mathcal{F}$, namely for

$$\mathcal{F}(U_1) = \mathcal{F}_{Cyl}^{kin,\Omega}(U_1) = \int_0^T \int_\Omega |U_1|^2 \, d\Omega \, dt \quad \text{and} \quad \mathcal{F}(U_1) = \mathcal{F}_{Cyl}^{rot,\Omega}(U_1) = \int_0^T \int_\Omega |\nabla \times U_1|^2 \, d\Omega \, dt,$$

$\nabla \times \cdot$ denoting the standard *curl* operator. In the first case we aim to control the kinetic energy of the fluid on the whole domain, while the vorticity of the flow on Ω is controlled for the second choice of $\mathcal{F}$.
For both the choices $\mathcal{F}_{Cyl}^{kin,\Omega}$ and $\mathcal{F}_{Cyl}^{rot,\Omega}$, either the primal solitary wave or the reflected one are crucial to control the target quantities. Indeed they are detected by the error estimator η_α and associated with the fine model. However, notice that the distribution of the mesh elements where the fine model (24) is solved (dark zones) changes according to the goal functional we are interested in.

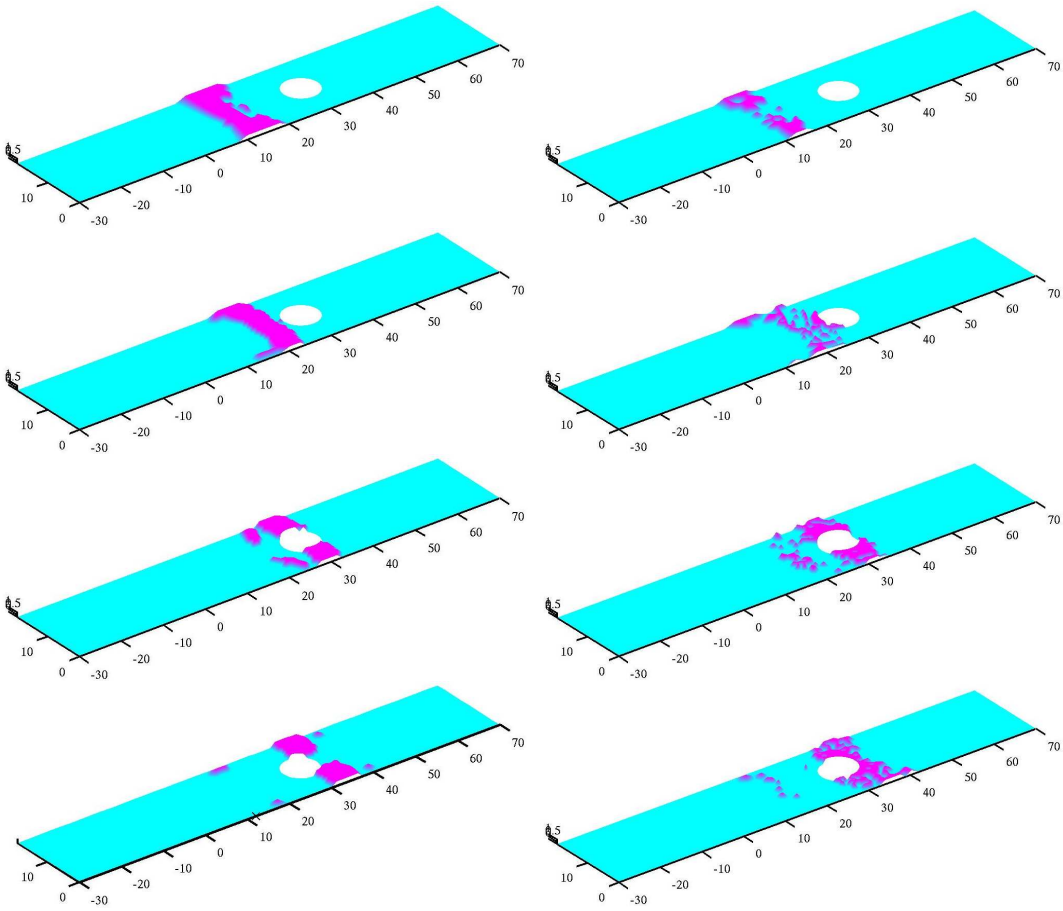

Figure 9: Distribution of the areas associated with the fine model (dark zones) and with the coarse model (light zones) for the channel with an obstacle test case and for the choices $\mathcal{F} = \mathcal{F}_{Cyl}^{kin,\Omega}$ (column on the left) and $\mathcal{F} = \mathcal{F}_{Cyl}^{rot,\Omega}$ (column on the right). Top-bottom: $t_j = 2s$, $6s$, $10s$ and $12s$

This test case has been used to assess the sensitivity of the numerical approximation with respect to the choice of the time step Δt and of the computational mesh. In more detail, we have evaluated the error estimator η_α by using the same computational grid (of $N_h = 1580$ triangles) and with the aim of approximating the goal quantity $\mathcal{F}_{Cyl}^{kin,\gamma}(U_1)$ with an accuracy $\tau = 10^{-3}$. Two different time steps have been adopted, $\Delta t = 0.1s$ and $\Delta t = 0.05s$, respectively. The corresponding distributions of the fine and coarse areas at four different times are represented in Fig. 10.
The number of triangles where the fine model (24) is solved is lower when the smaller Δt is adopted, even if the difference is not so relevant. As already inferred from the Gaussian hill test case, the choice of a small time step seems not to be a so convenient strategy. The increase of the computational effort associated with a smaller Δt is not balanced by a considerable reduction of the number of "fine triangles".

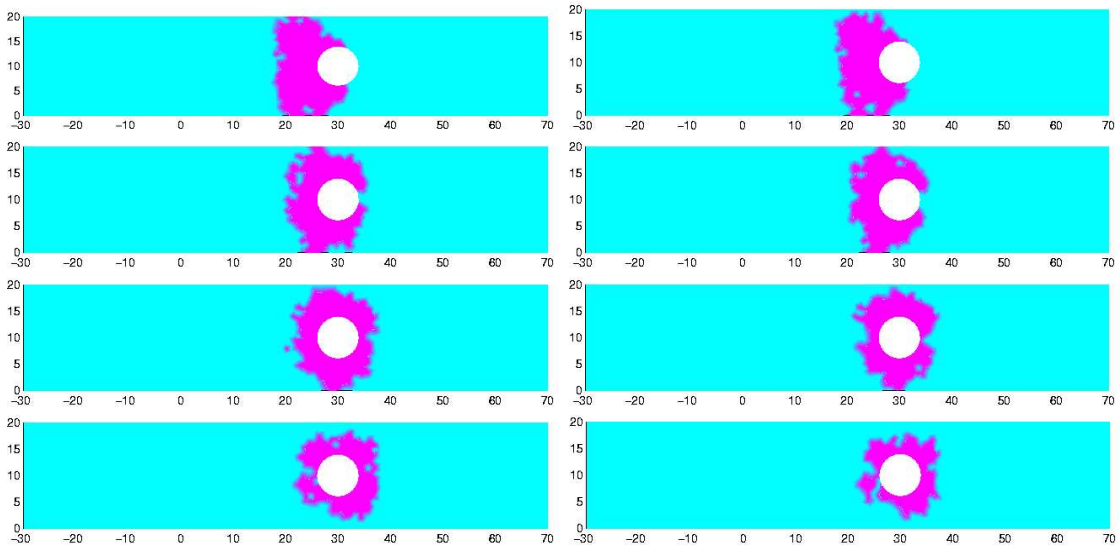

Figure 10: Comparison between the distributions of the "fine areas" (dark zones) and of the "coarse areas" (light zones) for the channel with an obstacle test case with $\mathcal{F} = \mathcal{F}_{Cyl}^{kin,\gamma}$ and for the choice $\Delta t = 0.1s$ (column on the left) and $\Delta t = 0.05s$ (column on the right). Top-bottom: $t_j = 6s$, $9s$, $10s$ and $12s$

A comparison of the time evolution of the quantity $\mathcal{F}_{Cyl}^{kin,\gamma}(U_\alpha)$ with the corresponding coarse and fine values $\mathcal{F}_{Cyl}^{kin,\gamma}(U_1)$ and $\mathcal{F}_{Cyl}^{kin,\gamma}(U_0)$, respectively is provided in Fig. 11, for the two choices $\Delta t = 0.1s$ (on the left) and $\Delta t = 0.05s$ (on the right). The three curves are characterized by the same trend. As expected, the kinetic energy estimated by the adapted model (dashed line) represents a more reliable prediction for the target quantity $\mathcal{F}_{Cyl}^{kin,\gamma}(U_1)$ (solid line) with respect to the values predicted by the coarse model (solid with circles line). Also in this case the difference due to the choice of the step size is minimum (it suffices to compare the two plots in Fig. 11).

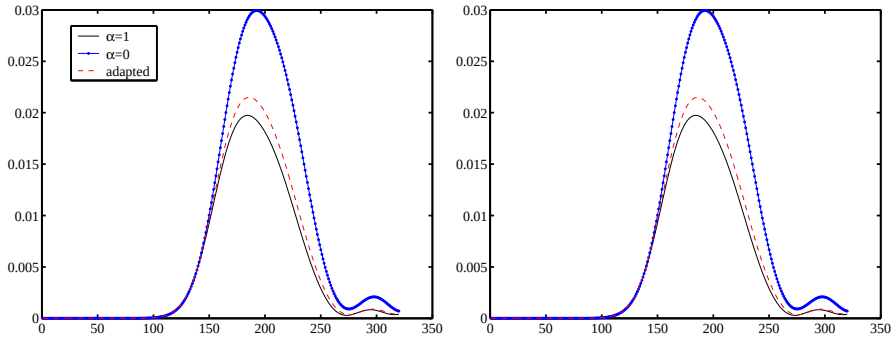

Figure 11: Evolution of the kinetic energy as a function of the time step for the coarse model (solid with circles line), for the fine model (solid line) and for the adapted one (dashed line) for the choices $\Delta t = 0.1s$ (on the left) and $\Delta t = 0.05s$ (on the right)

To analyze the influence of the chosen computational mesh on the evaluation of the modeling error estimator η_α, we have computed the quantity $\mathcal{F}_{Cyl}^{kin,\gamma}(U_\alpha)$ by using two different grids: the initial quasi-uniform mesh of $N_h = 2304$ elements on the left of Fig. 7 and a corresponding locally refined grid, obtained by refining the initial mesh only in a region around the obstacle, i.e. where the kinetic energy has to be controlled (see Fig. 7 on the right). The values $\tau = 10^{-3}$ and $\Delta t = 0.1s$ have been adopted for the tolerance and the time step, respectively.
The corresponding results are collected in Table 2.

τ	initial mesh	locally refined mesh
10^{-1}	$-5.6552 \cdot 10^{-1}$	$-1.4582 \cdot 10^{-1}$
10^{-2}	$-7.6179 \cdot 10^{-3}$	$-3.4512 \cdot 10^{-3}$
10^{-5}	$-2.2047 \cdot 10^{-5}$	$-1.1489 \cdot 10^{-6}$

Table 2: Sensitivity of the error estimator η_α with respect to the choice of the computational mesh for the channel with an obstacle test case

Notice that the order of magnitude of the quantities tabulated in the two columns is nearly the same, except when the tolerance τ is chosen equal to 10^{-5}. In such a case the employment of a suitably refined mesh turns out to be advantageous from a computational viewpoint.

5.2.3 The river bifurcation test case

As last benchmark, let us consider the propagation of a solitary wave along a river bifurcation. The reference computational domain $\Omega \subset \mathbb{R}^2$ is sketched in Fig. 12. It is a bifurcation $100m$ long, with a width at the inflow and at the two outflows equal to $10m$ and $7m$, respectively. The reference water level is equal to $5m$, while a flat bottom is assumed.

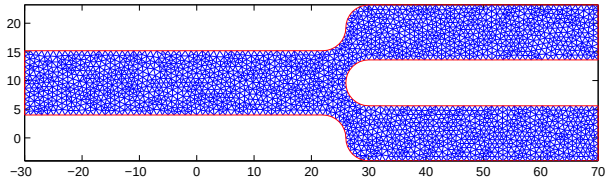

Figure 12: The river bifurcation test case: the quasi-uniform computational grid

The adapted model (23) is completed with exactly the same initial and boundary conditions adopted for the channel with an obstacle test case (see Section 5.2.2). Thus the solitary wave identified by the initial conditions (46) travels undisturbed, until it interacts with the bifurcation. Then a smaller reflected wave is generated.
The discrete scheme of Section 4 is applied moving from the computational grid in Fig. 12 consisting of $N_h = 7548$ elements and with a time step $\Delta t = 0.1s$, $T = 17s$ being the final time.

The nonlinear functional

$$\mathcal{F}(U_1) = \mathcal{F}_{Bif}^{kin,\Omega}(U_1) = \int_0^T \int_\Omega |U_1|^2 \, d\Omega \, dt$$

is selected as goal quantity, the tolerance τ being chosen equal to 10^{-2}.
Figure 13 provides us with the corresponding distribution of the areas where the fine and the coarse models are solved at times $t_j = 12s, 13s, 14s$ and $15s$. As expected, both the initial and the reflected waves are identified by the error estimator η_α as the main responsibles for controlling the kinetic energy of the fluid.

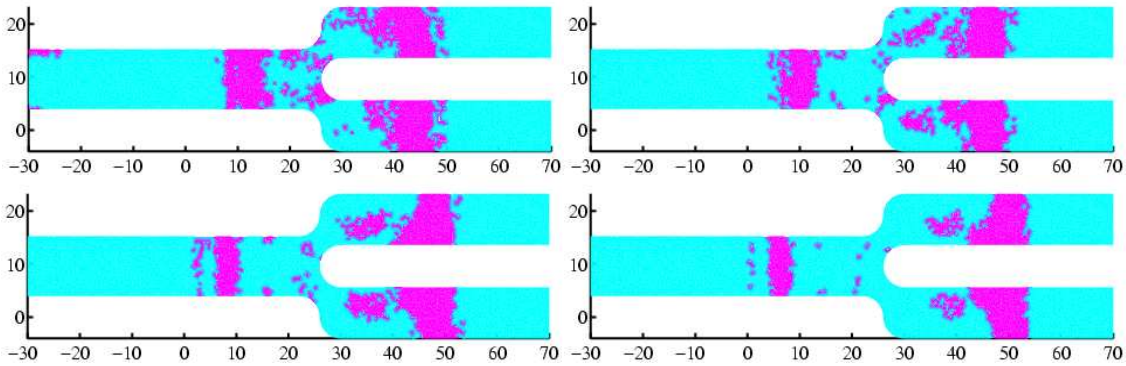

Figure 13: Distribution of the areas associated with the fine model (dark zones) and with the coarse model (light zones) for the river bifurcation test case. Left-right, top-bottom: $t_j = 12s$, $13s$, $14s$ and $15s$

Finally, we have repeated the same simulation by making a more restrictive requirement on the tolerance τ chosen equal to 10^{-3} and 10^{-4}, respectively. The corresponding values provided by the estimator η_α for the quantity $\mathcal{F}_{Bif}^{kin,\Omega}(U_1) - \mathcal{F}_{Bif}^{kin,\Omega}(U_\alpha)$ are gathered in Table 3. The accuracy demanded on the quantity η_α is largely guaranteed for each choice of τ.

τ	$\mathcal{F}_{Bif}^{kin,\Omega}(U_1) - \mathcal{F}_{Bif}^{kin,\Omega}(U_\alpha)$
10^{-2}	$-4.6506 \cdot 10^{-3}$
10^{-3}	$-1.9876 \cdot 10^{-4}$
10^{-4}	$8.8259 \cdot 10^{-7}$

Table 3: Sensitivity of the error estimator η_α with respect to the tolerance τ for the river bifurcation test case

Remark 5.3 *We recall that the solitary wave (46) assigned as initial condition for the two last test cases does not represent an analytical solution for the shallow water equations. As a consequence, besides the "physical" reflected wave due to the interaction of*

the solitary wave with the obstacle or with the bifurcation, a second small "non-physical" reflected wave will arise in both the simulations.

Remark 5.4 *A heuristic check of the regularity assumptions made to deduce the modeling error estimator (37) from the exact relation (36) has been performed in the case of the Gaussian hill and of the channel with an obstacle test case. In more detail, for these test cases we have compared the terms* (I) *and* (II) *in (36) (see Fig. 14). An order of magnitude separates the two terms almost everywhere in agreement with the considerations made above on the asymptotic behaviour of* (I) *and* (II).

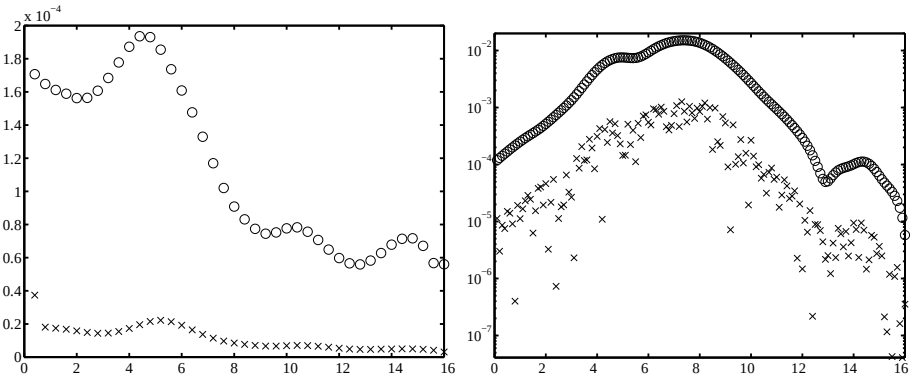

Figure 14: Comparison between the terms (I) (circles) and (II) (crosses) for the Gaussian hill (on the left) and for the channel with an obstacle (on the right) test case as a function of time

6 Conclusions

Moving from a hierarchy of hydrodynamic models, we provide in this paper an efficient tool to estimate the target quantity $\mathcal{F}(u_{fine})$, u_{fine} being the solution of the most complex model of such a hierarchy and where $\mathcal{F}$ denotes an output functional of interest. The leading idea is to evaluate $\mathcal{F}(u_{fine})$ within a prescribed accuracy by means of the quantity $\mathcal{F}(u_{adapted})$, where $u_{adapted}$ is the adapted solution, i.e obtained by limiting the solution of the most complex problem only to the areas of the computational domain that most influence the goal quantity. This aim is obtained thanks to a suitable *a posteriori* modeling error estimator developed in a goal-oriented framework.
The novelty of the analysis proposed in this paper consists of an extension of the approach provided in [3] to the case of time-dependent problems. The main difficulty related to unsteady problems is essentially the time discretization of the dual problem, as reverse time scales are involved. This unavoidably leads to a an increase of the computational cost. However this technique is still convenient when the increase of the computational cost, due to the resolution of the dual problem, is balanced by a considerable reduction of

the areas of the domain where the finest problem is solved. For instance, this is the case of complex hydrodynamic configurations, where an *a priori* "subdomain-to-model" correspondence is not always evident (see, [16]). Moreover this *a posteriori* analysis allows us to control physically meaningful functionals of the numerical solution in engineering applications.
The idea of an *a posteriori* modeling error estimator could be undoubtly more incisive when dimensionally heterogeneous–physically homogeneous models are coupled. This idea will be investigated in a forthcoming paper.

Appendix. Proof of Proposition 2.1. Let us consider the error on the goal quantity $\mathcal{F}(u_1) - \mathcal{F}(u_\alpha)$. Thanks to the relations (17) and (15) and by using the definition (16) of δL, we can rewrite it as

$$\begin{aligned} \mathcal{F}(u_1) - \mathcal{F}(u_\alpha) &= L(x_1) - L_\alpha(x_\alpha) = L(x_1) - L(x_\alpha) + \delta L(x_\alpha) \\ &= -d(u_\alpha)((1-\alpha)z_\alpha) + \int_0^1 L'(x_\alpha + \lambda e)(e)\, d\lambda\,. \end{aligned} \tag{47}$$

The trapezoidal rule applied to the integral in (47) yields

$$\int_0^1 L'(x_\alpha + \lambda e)(e)\, d\lambda = \frac{1}{2}\left\{L'(x_1)(e) + L'(x_\alpha)(e) + R\right\},$$

R being the remainder term defined in (21). Now, moving from equalities (5) and (15), and by exploiting the relation $L'_\alpha(x_\alpha)(y) = 0$, for any $y \in X$, we get

$$\begin{aligned} L'(x_1)(e) + L'(x_\alpha)(e) &= L'(x_\alpha)(e) = L'_\alpha(x_\alpha)(e) + \delta L'(x_\alpha)(e) \\ &= \delta L'(x_\alpha)(e) = -d(u_\alpha)((1-\alpha)e_z) - d'(u_\alpha)(e_u, (1-\alpha)z_\alpha), \end{aligned}$$

from which result (20) follows, after introducing the definitions (18) and (19) for the modeling residuals $\rho_M(u_\alpha)(z_\alpha)$, $\rho_M(u_\alpha)(e_z)$ and $\overline{\rho}_M(u_\alpha)(e_u, z_\alpha)$.

Acknowledgement

I thank Professor F. Saleri for carrying out the numerical computations and Professor A. Ern for his useful comments.

References

[1] R.L. Actis, B.A. Szabo and C. Schwab, *Hierarchic models for laminated plates and shells*, Comput. Methods Appl. Mech. Engrg., 172 (1999), pp. 79–107.

[2] R. Becker and R. Rannacher, *An optimal control approach to a posteriori error estimation in finite element methods*, in Acta Numerica 2001, A. Iserles, Eds., Cambridge University Press, Cambridge, UK, 2001.

[3] M. Braack and A. Ern, *A posteriori control of modeling errors and discretizatin errors*, Multiscale Model Simul., 1 No. 2 (2003), pp. 221–238.

[4] J.M. Cnossen, H. Bijl, B. Koren and E.H. van Brummelen, *Model error estimation in global functionals based on adjoint formulation*, in International Conference on Adaptive Modeling and Simulation, ADMOS 2003, N.-E. Wiberg and P. Díez, Eds., CIMNE, Barcelona, 2003.

[5] K. Eriksson, D. Estep, P. Hansbo and C. Johnson, *Computational Differential Equations*, Cambridge University Press, Cambridge, 1996.

[6] M. Feistauer and C. Schwab, *Coupling of an interior Navier-Stokes problem with an exterior Oseen problem*, J. Math. Fluid. Mech., 3 (2001), pp. 1–17.

[7] L. Formaggia, J.F. Gerbeau, F. Nobile and A. Quarteroni, *On the coupling of 3D and 1D Navier-Stokes equations for flow problems in compliant vessels*, Comput. Methods Appl. Mech. Engrg., 191 (2001), pp. 561–582.

[8] L. Formaggia, F. Nobile, A. Quarteroni and A. Veneziani, *Multiscale modelling of the circolatory system: a preliminary analysis*, Comput. Visual. Sci., 2 (1999), pp. 75-83.

[9] L. Formaggia and A. Quarteroni, *Mathematical Modelling and Numerical Simulation of the Cardiovascular System*, in Modelling of Living Systems, Handbook of Numerical Analysis, N. Ayache, P.G. Ciarlet, J.L. Lions, Eds., Elsevier Science, Amsterdam, to appear.

[10] M.B. Giles and N.A. Pierce, *Adjoint equations in CFD: duality, boundary conditions and solution behaviour*, AIAA Paper 97-1850 (1997).

[11] V. Girault and P.A. Raviart, *Finite Element Methods for Navier-Stokes Equations: Theory and Algorithms*, Springer Series in Computational Mathematics, Vol. 5, Springer-Verlag, Berlin, 1986.

[12] J.L. Lions and E. Magenes, *Non-Homogeneous Boundary Value Problems and Applications*, Volume I. Springer-Verlag, Berlin, 1972.

[13] G.I. Marchuk, V.I. Agoshkov and V.P. Shutyaev, *Adjoint equations and perturbation algorithms in nonlinear problems*, CRC Press, 1996.

[14] E. Miglio, S. Perotto and F. Saleri, *A multiphysics strategy for free-surface flows*, accepted for the publication in *Lecture Notes in Computational Sciences and Engineering*, Proceedings of the 15th International Conference on Domain Decomposition Methods, R. Kornhuber, R.H.W. Hoppe, D.E. Keyes, J. Periaux, O. Pironneau, J. Xu, Eds., Springer-Verlag 2003.

[15] E. Miglio, S. Perotto and F. Saleri, *On the coupling of 2D and 1D shallow water models for the simulation of free-surface flows*, in preparation (2004).

[16] E. Miglio, S. Perotto and F. Saleri, *Model coupling techniques for free-surface flow problems. Part I*, accepted for the publication in Proceedings of the Fourth World Congress of Nonlinear Analysis WCNA-2004, Orlando, Florida USA (2004).

[17] J.T. Oden and S. Prudhomme, *Estimation of modeling error in computational mechanics*, J. Comput. Phys., 182 (2002), pp. 469–515.

[18] J.T. Oden, S. Prudhomme, D.C. Hammerand and M.S. Kuczma, *Modeling error and adaptivity in nonlinear continuum mechanics*, Comput. Methods Appl. Mech. Engrg., 190 (2001), pp. 6663–6684.

[19] J.T. Oden and K.S. Vemaganti, *Estimation of local modeling error and goal-oriented adaptive modeling of heterogeneous materials. I. Error estimates and adaptive algorithms*, J. Comput. Phys., 164 No. 1 (2000), pp. 22–47.

[20] J.T. Oden and K.S. Vemaganti, *Estimation of local modeling error and goal-oriented adaptive modeling of heterogeneous materials. II. A computational environment for adaptive modeling of heterogeneous elastic solids*, Comput. Methods Appl. Mech. Engrg., 190 No. 46-47 (2001), pp. 6089–6124.

[21] A. Quarteroni and L. Stolcis, *Heterogeneous domain decomposition for compressible flows*, in Proceedings of the ICFD Conference on Numerical Methods for Fluid Dynamics, M. Baines and W.K. Morton, Eds., Oxford University Press, Oxford, 1995, pp. 113-128.

[22] A. Quarteroni and A. Valli, *Domain decomposition methods for partial differential equations*, Oxford University Press Inc., New York, 1999.

[23] M. Schulz and G. Steinebach, *Two-dimensional modelling of the river Rhine*, J. Comput. Appl. Math., 145 No. 1 (2002), pp. 11–20.

[24] E. Stein and S. Ohnimus, *Anisotropic discretization- and model-error estimation in solid mechanics by local Neumann problems*, Comput. Methods Appl. Mech. Engrg., 176 (1999), pp. 363–385.

[25] C.B. Vreugdenhil, *Numerical Methods for Shallow-Water Flows*, Kluwer Academic Press, Dordrecht, 1998.

[26] G.B. Whitham, *Linear and Nonlinear Waves*, Wiley, New York, 1974.